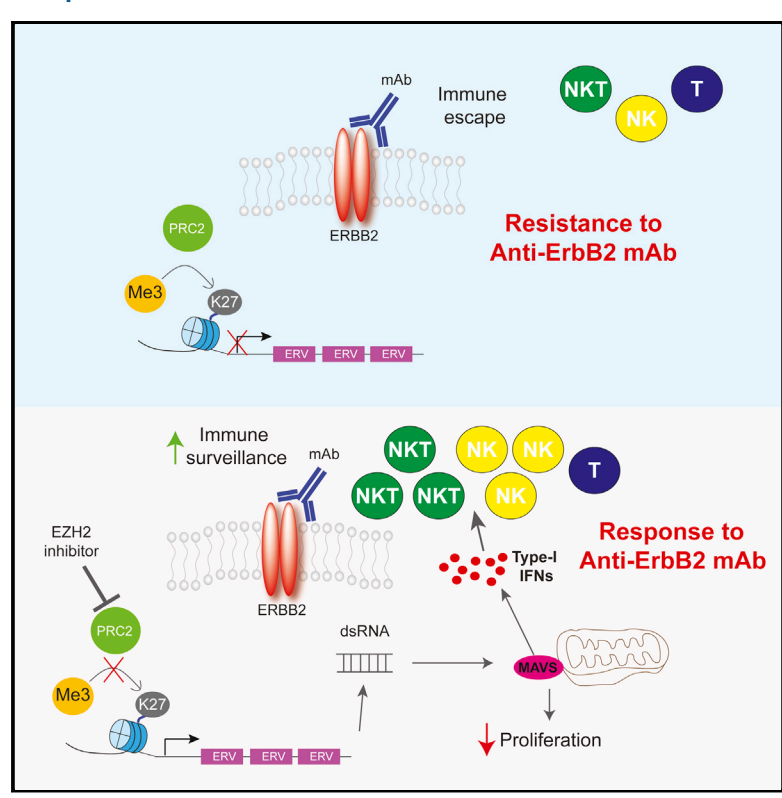
Cell Reports

Reduction of Global H3K27me³ Enhances HER2/ ErbB2 Targeted Therapy

Graphical Abstract



Highlights

- EZH2 activity correlates with Trastuzumab resistance and antiviral gene silencing
- EZH2 silences retrotransposons in ErbB2+ breast cancer
- EZH2 inhibition induces retrotransposon expression and a type-I interferon response
- Inhibiting EZH2 in vivo boosts immune infiltration and response to anti-ErbB2 mAbs

Authors

Alison Hirukawa, Salendra Singh, Jarey Wang, ..., Vinay Varadan, Harvey W. Smith, William J. Muller

Correspondence

harvey.smith2@mcgill.ca (H.W.S.), william.muller@mcgill.ca (W.J.M.)

In Brief

Hirukawa et al. link Trastuzumab resistance in ErbB2+ breast cancers with activity of the methyltransferase EZH2, a key epigenetic regulator. By silencing retrotransposons, EZH2 suppresses type-I interferon signaling to limit immune surveillance. Retrotransposon derepression following EZH2 inhibition triggers interferon responses and sensitizes immunocompetent *in vivo* models to ErbB2 antibody therapy.









Reduction of Global H3K27me³ Enhances HER2/ErbB2 Targeted Therapy

Alison Hirukawa, 1,2 Salendra Singh,3 Jarey Wang,4 Jonathan P. Rennhack,5 Matthew Swiatnicki,5

Virginie Sanguin-Gendreau,^{1,2} Dongmei Zuo,^{1,2} Kamilia Daldoul,^{1,2} Cynthia Lavoie,^{1,2} Morag Park,^{1,6} Eran R. Andrechek,⁵ Thomas F. Westbrook,^{4,7} Lyndsay N. Harris,^{3,8} Vinay Varadan,³ Harvey W. Smith,^{1,9,10,*} and William J. Muller^{1,2,9,11,*}

SUMMARY

Monoclonal antibodies (mAbs) targeting the oncogenic receptor tyrosine kinase ERBB2/HER2, such as Trastuzumab, are the standard of care therapy for breast cancers driven by ERBB2 overexpression and activation. However, a substantial proportion of patients exhibit de novo resistance. Here, by comparing matched Trastuzumab-naive and posttreatment patient samples from a neoadjuvant trial, we link resistance with elevation of H3K27me³, a repressive histone modification catalyzed by polycomb repressor complex 2 (PRC2). In ErbB2+ breast cancer models, PRC2 silences endogenous retroviruses (ERVs) to suppress anti-tumor type-I interferon (IFN) responses. In patients, elevated H3K27me³ in tumor cells following Trastuzumab treatment correlates with suppression of interferon-driven viral defense gene expression signatures and poor response. Using an immunocompetent model, we provide evidence that EZH2 inhibitors promote interferon-driven immune responses that enhance the efficacy of anti-ErbB2 mAbs, suggesting the potential clinical benefit of epigenomic reprogramming by H3K27me³ depletion in Trastuzumab-resistant disease.

INTRODUCTION

The anti-ERBB2 monoclonal antibody (mAb) Trastuzumab has revolutionized the treatment of ERBB2+ cancers, including approximately 20% of mammary tumors. However, even in com-

bination with cytotoxic chemotherapy, responses to Trastuzumab are limited by primary (de novo) and acquired resistance in most cases (Rimawi et al., 2015). In keeping with clinical correlations between pathological complete response (pCR) to anti-cancer therapies in the neoadjuvant setting and overall survival, primary resistance to neoadjuvant Trastuzumab in ERBB2+ breast cancer is associated with a particularly poor outcome (Mayer et al., 2015). However, the molecular mechanisms responsible for de novo Trastuzumab resistance remain incompletely characterized. While most studies have focused on modifications and protein-protein interactions involving ERBB2 or co-operating genetic events constitutively activating downstream pathways (Loibl et al., 2014; Majewski et al., 2015; Wilken and Maihle, 2010), Trastuzumab is thought to act largely through the host immune system, eliciting antibodydependent cellular cytotoxicity (ADCC) to eliminate ERBB2+ tumor cells (Clynes et al., 2000; Mimura et al., 2005; Spiridon et al., 2002). Overall, there is an urgent need to improve the understanding of mechanisms promoting Trastuzumab resistance, with a view to improving clinical outcomes for patients with aggressive, ERBB2+ breast cancers.

Alterations in the patterns of chemical modifications of DNA and histones can perturb transcriptional programs affecting cellular identity and are well-established drivers of many cancers. Epigenetic reprogramming can also mediate resistance to targeted therapies (Scott et al., 2016; Sharma et al., 2010). However, few studies have examined the role of epigenetic regulation in Trastuzumab resistance. Among the most prominent epigenetic modifiers implicated in ERBB2+ breast cancer is polycomb repressor complex 2 (PRC2) (Holm et al., 2012; Kleer et al., 2003), containing the methyltransferase subunit EZH2, which targets lysine 27 of histone H3 to repress transcription. PRC2 exerts context-dependent oncogenic and tumor-suppressive functions in various tumor types. In breast cancer, EZH2 overexpression is well documented in aggressive subtypes,



¹Rosalind and Morris Goodman Cancer Research Centre, McGill University, Montréal, QC H3A 1A3, Canada

²Department of Biochemistry, McGill University, Montréal, QC H3A 1A3, Canada

³Case Comprehensive Cancer Center, Case Western University, Cleveland, OH 44145, USA

⁴Verna and Marrs McLean Department of Biochemistry and Molecular Biology, Baylor College of Medicine, Houston, TX 77030, USA

⁵Department of Physiology, Michigan State University, East Lansing, MI 48824, USA

⁶Departments of Medicine and Oncology, McGill University, Montréal, QC H3A 1A3, Canada

⁷Department of Molecular and Human Genetics, Interdepartmental Program in Molecular and Biomedical Sciences, Dan L. Duncan Cancer Center, Department of Molecular and Cellular Biology, and Therapeutic Innovation Center, Baylor College of Medicine, Houston, TX 77030, USA

⁸Division of Cancer Treatment and Diagnosis, National Cancer Institute, NIH, Rockville, MD 20892, USA

⁹Senior author

¹⁰Twitter: @Harvey_W_Smith

¹¹Lead Contact

^{*}Correspondence: harvey.smith2@mcgill.ca (H.W.S.), william.muller@mcgill.ca (W.J.M.) https://doi.org/10.1016/j.celrep.2019.08.105



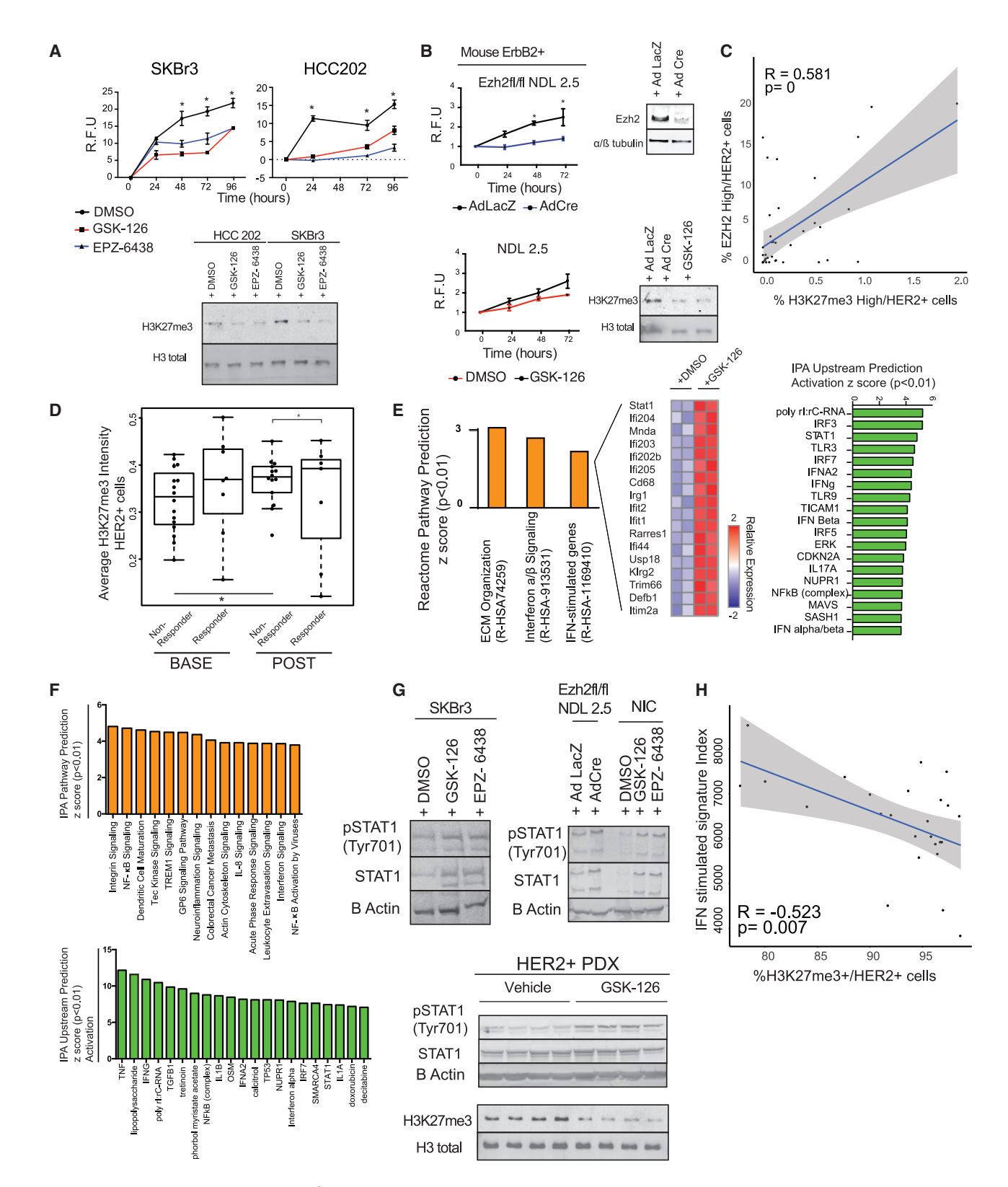


Figure 1. Depletion of Global H3K27me³ in ERBB2+ Breast Cancer Induces a Type-I Interferon Response and Correlates with Patient Response to ERBB2 Targeted Therapy

(A) Proliferation of ERBB2+ cell lines treated with DMSO, GSK126 (2 µM), or EPZ-6438 (2 µM) for 72 h prior to initiation of the assay (representative of four independent experiments). H3K27me³ levels were assessed by immunoblotting (bottom panel).

including ERBB2+ tumors, where it correlates with the abundance of tri-methylation on H3K27 (H3K27me³) (Holm et al., 2012). However, the precise mechanisms by which PRC2 contributes to ERBB2-driven mammary tumorigenesis are unclear, and any potential function of PRC2 in resistance to ERBB2-targeted therapies, including Trastuzumab, is unknown.

In this study, we have combined analysis of breast cancer patient samples with *in vitro* and *in vivo* functional studies to demonstrate that PRC2 significantly attenuates the response to anti-ErbB2 mAb therapy. We identify silencing of retrotransposons—in particular, endogenous retroviruses (ERVs)—as a critical function of PRC2 in ERBB2+ breast cancers. EZH2 inhibitors, which are currently progressing through clinical trials in multiple tumor types, de-repress these transposable elements to impair tumor cell proliferation and trigger anti-tumor immune responses through the activation of a type-I interferon (IFN) response. These findings reveal an important mechanism mediating resistance to anti-ERBB2 mAbs and delineate a strategy for improving the clinical response to these important therapies.

RESULTS

Upregulation of PRC2 Activity in Trastuzumab-Resistant ERBB2+ Breast Cancers

We recently found that Ezh2 is essential for ErbB2-dependent transformation of the mammary epithelium in vivo, while upregulation of Ezh2 protein expression drives ErbB2+ tumor cell growth (Smith et al., 2019). To examine the role of PRC2 in breast cancer cells, we treated a panel of cell lines corresponding to various molecular subtypes (Luminal/ERα+, ERBB2+, and triple-negative breast cancer) with two independent EZH2 inhibitors. Supporting a role for H3K27me³ in ERBB2+ breast cancer, EZH2 inhibition significantly attenuated the proliferation of multiple ERBB2+ breast cancer cell lines at published concentrations (0.5-5 µM; Bitler et al., 2015; Huang et al., 2018b; Kim et al., 2015; Knutson et al., 2013), consistent with the reported plasma C_{max} of Ezh2 inhibitors in patients (Italiano et al., 2018), in a manner correlating with H3K27me³ loss (Figures 1A, S1, and S2A). Furthermore, deletion or inhibition of Ezh2 blocked proliferation in ErbB2-driven primary mouse mammary tumor cells (Figures 1B, S2B, and S2C). To determine the clinical relevance of these observations, we examined tumor-cell-specific H3K27me³ levels and EZH2 protein expression in patient samples (Figure S2D). We confirmed a positive correlation between tumor-cell-specific H3K27me³ and EZH2 levels, as observed previously (Holm et al., 2012) (Figure 1C). To determine whether PRC2 was implicated in the response to Trastuzumab, we compared H3K27me³ levels in matched core biopsies of ERBB2+ breast cancers obtained prior to and following neoadjuvant Trastuzumab (Varadan et al., 2016a), correlating changes in H3K27me³ with clinical response. Strikingly, post-treatment samples from Trastuzumab non-responsive tumors had significantly elevated tumor-cell-specific H3K27me³ compared to the baseline, potentially implicating PRC2 activity in Trastuzumab resistance (Figure 1D; p < 0.05).

PRC2 Inhibition Triggers a Type-I Interferon Response in ErbB2+ Breast Cancer Cells

To identify PRC2-regulated gene expression programs implicated in resistance to anti-ErbB2 mAbs, we treated ErbB2+ breast cancer cells with the Ezh2 methyltransferase inhibitor GSK126 and performed transcriptomic profiling. We identified 782 differentially expressed mRNAs enriched in signatures of IFN α/β signaling and predicted to be downstream of IFN α/β regulators such as MAVS and TLR3 (Figure 1E). The induction of a type-I interferon response upon depletion of global H3K27me³ was also observed in human ERBB2+ breast cancer cells (Figure 1F). We validated increased mRNA expression of representative type-I interferon response-related genes following a loss of Ezh2 function (Figures S3A and S3B). Accordingly, IFNα/β secretion and STAT1 phosphorylation were elevated in GSK126-treated ERBB2+ breast cancer cell lines and ERBB2+ patient-derived xenograft (PDX) tumors (Figures 1G, S3C, and S3D). By linking RNA sequencing (RNA-seq) and immunofluorescence data from therapy-naive and post-treatment biopsies, we observed a negative correlation between H3K27me³ and interferon-stimulated gene expression at baseline in the clinical setting (Figure 1H). Trastuzumab-responsive tumors also exhibited an increased expression of established viral defense (Chiappinelli et al., 2016a) and interferon-regulated

⁽B) Proliferation of Ezh2^{fl/fl} or Ezh2^{fl/fl} er Ezh2^{fl/fl} ErbB2+ transgenic mouse mammary tumor cells infected with adenoviruses bearing Cre recombinase or LacZ 96 h prior to the assay, or treated with Ezh2 inhibitors or DMSO as in (A). H3K27me³ levels were assessed by immunoblotting (bottom panel). Data in (A) and (B) are mean \pm SEM, *p < 0.05, one-way ANOVA with Tukey's post-test.

⁽C) Pearson's correlation analysis of EZH2 and H3K27me³ levels in core tumor biopsies from patients with stage II–III ERBB2+ breast cancer. High signal denotes samples that scored 3+.

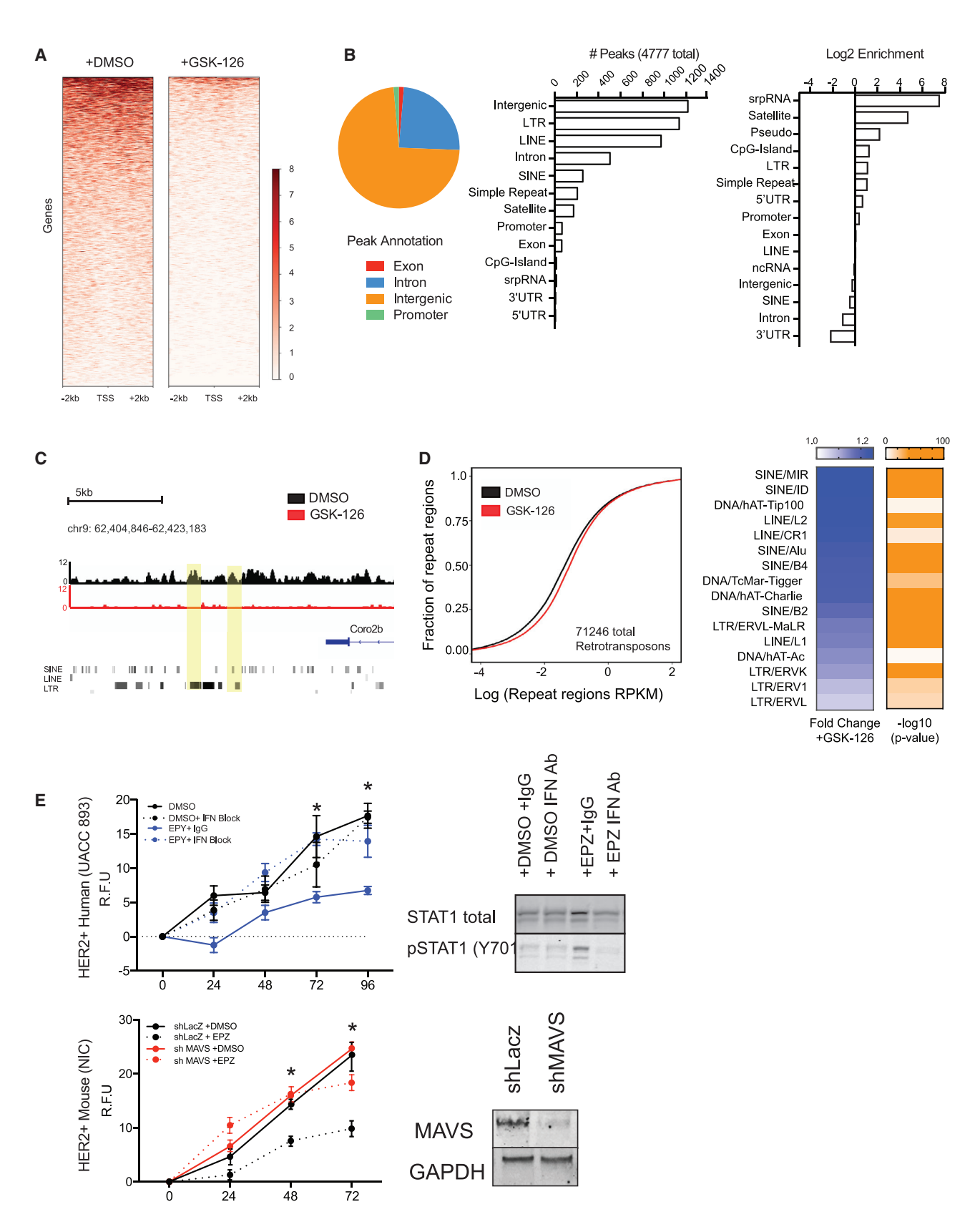
⁽D) Immunofluorescence analysis of H3K27me 3 in ERBB2+ tumor cells in patient core biopsies prior to (Base) and 14 days after (Post) a loading dose of Trastuzumab (8 mg/kg given prior to switching to the maintenance dose [2 mg/kg] for the duration of treatment). Upper and lower whiskers indicate maximum and minimum values, box boundaries indicate first and third quartiles, and horizontal line indicates the median. *p < 0.05, unpaired Student's t test.

⁽E) Gene expression profiling of ErbB2+ transgenic mouse mammary tumor cells (NIC) treated with GSK126 or DMSO for 7 days. Left panel: predicted active pathways (Reactome) in GSK126-treated cells. Middle panel: differential expression of genes in the interferon (IFN)-stimulated gene signature (Reactome). Right panel: IPA (ingenuity pathway analysis) of upstream transcriptional regulators of differentially expressed genes in GSK126-treated cells. The activation Z score infers the activation state of each predicted transcriptional regulator. Data are representative of two independent experiments.

⁽F) Gene expression profiling of ERBB2-driven human cell lines (SkBr3) treated with GSK126 or DMSO for 7 days. Top panel: IPA of pathways enriched in SkBr3 cells treated with GSK126. Bottom panel: factors predicted by IPA upstream regulator analysis. Data are representative of two independent experiments. (G) Immunoblot of total and phosphorylated (Y701) STAT1. Top panels: SkBr3 and NIC cells treated with DMSO, GSK126 (2 μM), or EPZ-6438 (2 μM) for 7 days, or Ezh2^{fl/fl} NDL2.5 treated with adenovirus expressing LacZ or Cre recombinase for 96 h. Bottom panel: data from endpoint ERBB2+ PDX tumors treated with vehicle or GSK126 *in vivo*.

⁽H) Pearson's correlation analysis of the interferon-stimulated gene signature (Figure 1E) and H3K27me³ levels in ERBB2+ breast cancer patient core biopsies. See also Figures S1–S3.





gene expression signatures compared to non-responsive tumors (Figures S3E and S3F). Collectively, these data suggest that PRC2 opposes an interferon response involved in mediating responsiveness to Trastuzumab.

PRC2 Suppresses Retrotransposon Expression in ErbB2+ Breast Cancer Cells

Repressive epigenetic modifications can dampen the efficacy of immunotherapies by silencing genes involved in cytokine responses (Peng et al., 2015). Genome-wide profiling of ErbB2+ cells (Figure 2A) revealed a loss of H3K27me3 upstream of the transcription start site (TSS) for 9% of genes upregulated by GSK126 treatment (Figures 2B and S4A). Cross-correlation of RNA-seq and chromatin immunoprecipitation sequencing (ChIP-seq) data revealed that key genes in the type-I interferon pathway (e.g., Stat1, Ifit2) and signatures associated with the Trastuzumab response (Kauraniemi et al., 2004; Végran et al., 2009) were not directly repressed by PRC2. Interestingly, type-I interferon genes did exhibit H3K27me³ peaks near their promoters (Figures S4B-S4D), suggesting that their de-repression may contribute to the induction of a type-I interferon response upon Ezh2 inhibition in ErbB2+ cells. However, in agreement with studies of other cell types (Ishak et al., 2016), H3K27me³ deposition in ErbB2+ cells occurred mainly in introns and intergenic regions, including genomic repeat elements (Figures 2B and 2C). We identified differential expression of 294 retrotransposon families in GSK126-treated cells compared to controls, with 85% being upregulated (Figure 2D; Table S1). Prominent among these were ERVs, the transcription of which generates double-stranded RNA (dsRNA) that activates cytosolic sensors to trigger type-I interferon signaling via the mitochondrial protein MAVS (Yoneyama et al., 2015). Deep RNA sequencing of GSK126-treated ERBB2+ PDX samples also revealed a significant upregulation of specific ERV families (Figure S5A). Although DNA methylation is also important in silencing ERVs (Chiappinelli et al., 2016a; Roulois et al., 2015), the expression of ERVs marked by H3K27me³ was not induced by the inhibition of DNA methylation using 5'-Aza-2-deoxycytidine (decitabine) (Figures S5B and S5C). Consistent with PRC2-dependent regulation of dsRNA sensing and type-I interferon signaling, IFNα/β blocking antibodies or silencing of MAVS rescued the proliferation of GSK126-treated cells and reduced STAT1 phosphorylation (Figure 2E).

Anti-ErbB2 mAb Therapy Is Enhanced by Ezh2 Inhibition in an Immunocompetent ErbB2+ Breast Cancer Model

Type-I interferon responses can elicit powerful anti-tumor effects through tumor-cell-autonomous mechanisms and by enhancing immune surveillance (Snell et al., 2017). In light of our observations, and given that the immune system dictates responses to anti-ErbB2 mAb therapy via ADCC (Clynes et al., 2000; Mimura et al., 2005; Spiridon et al., 2002), we hypothesized that EZH2 inhibition would improve responses to anti-ErbB2 mAbs. To determine whether GSK126 could enhance the efficacy of ErbB2 mAb therapy, we used an immunocompetent, orthotopic ErbB2+ allograft model and the anti-ErbB2 mAb clone 7.16.4, which recognizes an epitope of rodent ErbB2 that overlaps with the Trastuzumab-binding epitope of ERBB2 (Zhang et al., 1999) and can be recognized by Fc receptor-expressing murine immune cells. In two preclinical trials employing independently derived cell lines, combined 7.16.4 mAb/GSK126 treatment significantly attenuated tumor growth and elevated tumor cell apoptosis, compared to all other groups (Figures 3A-3C and S6A). Interestingly, combined 7.16.4 mAb/GSK126 treatment did not alter PI3K or extracellular signal-regulated kinase (ERK) pathway activation (Figure S6B), but it elicited the highest levels of STAT1 phosphorylation (Figure 3D), suggesting the strongest induction of an interferon-driven immune response. These data are consistent with an enhanced response to 7.16.4 mAb/ GSK126 therapy via non-tumor-cell-autonomous mechanisms, rather than effects on canonical ErbB2 signaling. Supporting the involvement of the immune system, GSK126 could not sensitize a resistant ERBB2+ PDX to anti-ERBB2 antibody therapy (4D5) in immunocompromised hosts (Figure S6C). In immunocompetent hosts, IFNy levels were elevated in GSK126 and 7.16.4 mAb/GSK126-treated tumors, consistent with leukocyte recruitment (Figure S6D). Furthermore, inhibition of EZH2 in breast cancer cell lines in vitro did not influence the response to anti-ErbB2 mAbs (Figure S7), regardless of whether the cells were initially sensitive to anti-ErbB2 mAbs (SkBr3) or de novo resistant (NIC and HCC1954). These data are consistent with a critical role for the immune system in the response to EZH2 inhibitor/anti-ErbB2 mAb combination therapy. We confirmed that while the recruitment of CD4+ and CD8+ T cells was unaffected, natural killer T (NKT) cell infiltration was significantly increased by 7.16.4 mAb/GSK126 treatment (15.3% of CD45+ immune cells versus <1% in other groups). Interestingly, infiltration of

Figure 2. H3K27me³ Peaks Are Enriched in Genomic Repeat Regions in ERBB2+ Breast Cancer Cells

(A) Heatmap showing H3K27me³ distribution within a -2 kb/+2 kb window centered on the TSS in ErbB2+ cells treated with DMSO or GSK126 (2 μM).

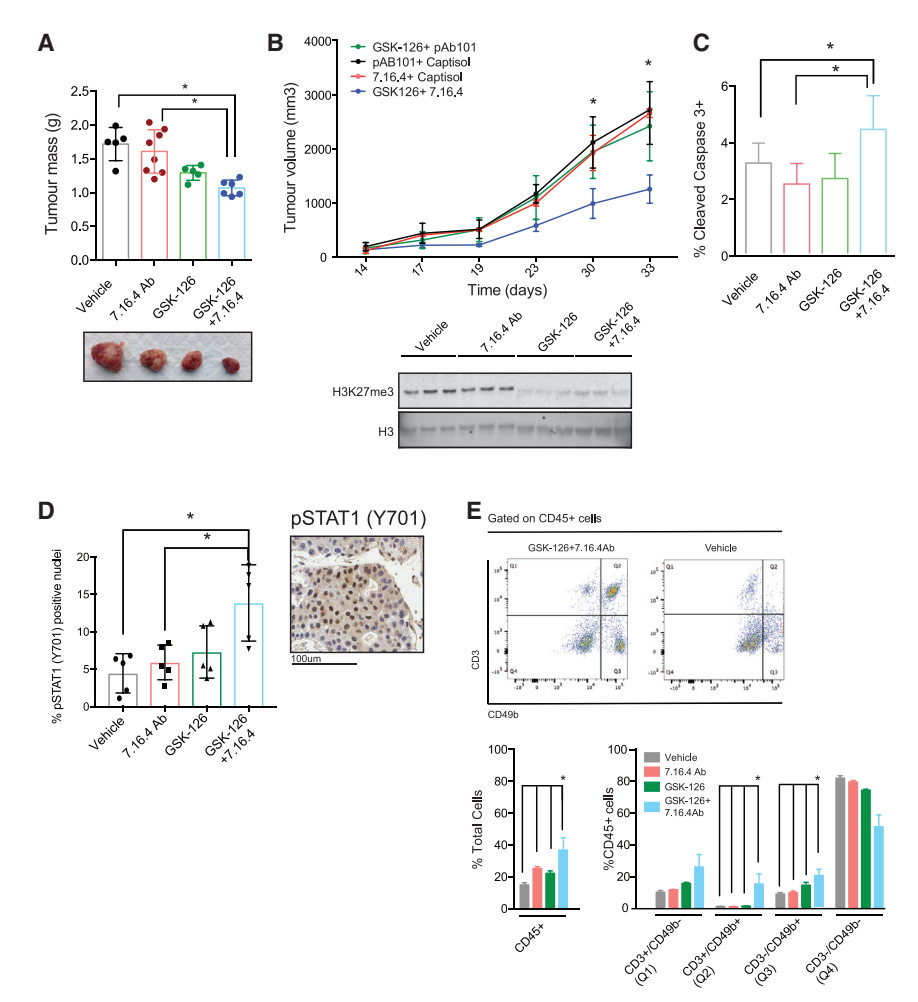
(B) Left panel: annotation of H3K27me³ sites in ErbB2+ cells. Middle panel: detailed annotation of H3K27me³ peaks further segregated by repeat elements. Right panel: enrichment of peaks in different genomic regions normalized to their occurrence. LTR, long terminal repeat; LINE, long interspersed element; SINE, short interspersed elements.

(C) University of California, Santa Cruz (UCSC) Genome Browser track showing H3K27me3 in DMSO- (black) or GSK126- (red) treated NIC cells overlaid with repeat regions from Repeat Masker. Yellow bar highlights coincidence of H3K27me3 peaks with LTR regions.

(D) Fraction of retrotransposons plotted against the log expression of the reads per kilobase of transcript per million reads (RPKM) in GSK126-treated (2 µM, 72 h) (red line) versus DMSO-treated (black line) NIC cells (left panel). Right panel: differential retrotransposon expression (blue) and -log10 p value (orange) following treatment with GSK126 (2 μ M, 72 h)

(E) Top panel: proliferation of ERBB2+ tumor cells (UACC 893) treated with DMSO or EPZ-6438 (2 µM for 5 days prior to the assay) and IgG or type-I interferon neutralizing antibody cocktail. Immunoblots showing STAT1 phosphorylation were performed at 96 h post-treatment. Bottom panel: proliferation of ErbB2+ primary mouse mammary tumor cells with shRNA-mediated silencing of MAVS in the presence or absence of DMSO or EPZ-6438 (2 µM). MAVS knockdown was assessed by immunoblot. Data are mean ± SEM, *p < 0.05, one-way ANOVA with Tukey's post-test. See also Figures S4 and S5.





NK cells was also significantly increased in 7.16.4 mAb/GSK126treated tumors (21.1%) and GSK126-treated tumors (16.7%), compared to other groups (6.8%, 7.2%) (Figure 3E). Collectively, these findings suggest that de-repression of retrotransposons by EZH2 inhibition triggers a type-I interferon response and an influx of cytotoxic leukocytes that potentiates the anti-tumor response to anti-ErbB2 mAb therapy.

DISCUSSION

Genomic repeat regions play various roles in cancer cells, including the regulation of proximal gene expression and activation of antiviral responses (Chiappinelli et al., 2016a; Roulois et al., 2015). Here, we have combined multimodal analysis of patient samples with preclinical models to show that PRC2 suppresses ERV expression and type-I interferon signaling in ErbB2+ breast cancer, promoting resistance to anti-ErbB2 mAb therapy. These findings indicate a possible strategy to improve primary responses in patients whose tumors are refractory to such treatment. Importantly, modification of the stromal epigenome, including that of immune cells, by systemic EZH2 inhibition may elicit a complex response. For example, EZH2 is an important determinant of T cell differentiation and survival

Figure 3. Global Reduction of H3K27me3 Enhances the Response of ERBB2 Monoclonal Antibodies to Dampen Tumor Progression

Immunocompetent mice bearing orthotopic ErbB2+ breast cancer allografts were treated with Captisol (vehicle) + pAb101 (control Ab), 7.16.4 Ab + Captisol, GSK126 + pAb101, or 7.16.4 Ab + GSK126 (n = 5 per condition).

- (A) Tumor mass was assessed at endpoint. Bottom panel shows representative images of endpoint tumors from each treatment group.
- (B) Tumor volume assessment at the indicated times during treatment (mean ± SEM, *p < 0.05. one-way ANOVA with Tukey's post-test). H3K27me3 levels in endpoint tumors were assessed by immunoblot (bottom panel).
- (C) Quantification of cleaved caspase 3 by immunohistochemistry in endpoint tumors.
- (D) Quantification of phospho-STAT1 (Y701) by immunohistochemistry in endpoint tumors.
- (E) Quantification of CD45+ cells and the percentage of T cells (CD3+/CD49b-), NKT cells (CD3+/ CD49b+), and NK cells (CD3-/CD49b+) among CD45+ hematopoietic cells in endpoint tumors (n = 5 per condition).

Data in (C)-(E) are mean \pm SEM, *p < 0.05, unpaired Student's t test versus vehicle control. See also Figures S6 and S7.

(Tong et al., 2014; Tumes et al., 2013; Zhao et al., 2016). While such effects may explain the absence of an increased T cell infiltrate in our in vivo studies, we note that the T cell population was not decreased relative to vehicle controls. However, chronic type-I interferon

signaling can also exhaust T cells (Benci et al., 2016; Yang et al., 2014), which may necessitate the modification of dosing strategies to activate immune surveillance without impairing T cell effector function. The infiltration of 7.16.4 mAb/GSK126treated tumors by NKT and NK cells is in accordance with their anti-tumor roles, including their ability to engage in ADCC (Ochoa et al., 2017), and their recruitment and activity in ErbB2+ cancers (Arnould et al., 2006; Park et al., 2018), where their presence may correlate with a good outcome (Finak et al., 2008). Notably, ongoing clinical trials are investigating strategies involving anti-ErbB2 mAbs with improved binding to NK cell Fc receptors (Huang et al., 2018a) or combining autologous NK cell infusion with Trastuzumab (Yadav et al., 2019). Our data are consistent with studies showing that Ezh2 loss enhances the development and cytotoxicity of NK cells (Yin et al., 2015) and stabilizes PLZF, a regulator of NKT cell identity, leading to an expansion of the NKT cell population (Vasanthakumar et al., 2017; Dobenecker et al., 2015). Anti-tumor immune responses induced by EZH2 inhibition may also improve the treatment of tumors with heterogeneous ERBB2 gene amplification and overexpression, where the expansion of ERBB2-negative populations is associated with a poor response to Trastuzumab (Lee et al., 2014; Vance et al., 2009).

Methylation of DNA and lysine 9 on histone H3 (H3K9me³) are considered the principal modes of repeat element silencing in mammalian cells. However, we and others have found that retrotransposons can also be marked by H3K27me³ (Ishak et al., 2016; Walter et al., 2016) and expressed upon a loss of PRC2 function (Groh and Schotta, 2017; Leeb et al., 2010). Furthermore, DNA methylation and H3K27me³ are mutually exclusive in some cell types, including some ERBB2+ breast cancer cells (Hon et al., 2012). Thus, the appropriate epigenetic regulator that can be targeted as part of a combination strategy to enhance anti-tumor immunity is likely to vary based on tumor type. Nucleoside analogs that inhibit DNA methylation can trigger ERV transcription and a type-I interferon response in ovarian and colon cancer cells (Chiappinelli et al., 2016a; Roulois et al., 2015) and are being explored in combination with immunotherapies (Chiappinelli et al., 2016b). However, their use for treating solid tumors is restricted by unfavorable pharmacokinetics and dose-limiting toxicity (Ahuja et al., 2014), and their ability to improve responses to mAbs or immunotherapies may be limited by an impairment of leukocyte differentiation and function (Gao et al., 2009; Niu et al., 2018; Wang et al., 2017). EZH2 inhibitors are progressing through multiple clinical trials, are well tolerated, and have shown efficacy in solid tumors (Italiano et al., 2018; Taplin et al., 2018). Our findings suggest that EZH2 inhibition may potentiate anti-tumor immunity in cancers where PRC2 silences ERVs and suppresses type-I interferon responses, such as ErbB2+ breast cancer. This may indicate a role for PRC2 targeting in combination with anti-ErbB2 mAbs as a strategy to improve responses and combat resistance, leading to better outcomes for patients with aggressive, ERBB2+ disease.

STAR*METHODS

Detailed methods are provided in the online version of this paper and include the following:

- KEY RESOURCES TABLE
- LEAD CONTACT AND MATERIALS AVAILABILITY
- EXPERIMENTAL MODEL AND SUBJECT DETAILS
 - Animal Models
 - Human Subjects
 - $\, \bigcirc \,$ Primary Cell Cultures and Cell Lines
 - Human cell lines
- METHOD DETAILS
 - *In vitro* experiments
 - O Lentiviral Production and Transduction
 - O Adenovirus Infection
 - Transcriptional Profiling Microarray
 - O Transcriptional Profiling RNA Sequencing
 - Chromatin Immunoprecipitation (ChIP)
 - O Analysis of Gene Expression Data
 - O CHIP-Seq Analysis
 - RNA-Seq Analysis
 - O Viral Defense Gene Expression Signature
 - O Retrotransposon expression analysis
 - ELISA
 - Flow cytometry
 - O Protein Extraction and Immunoblotting

- Immunofluorescence and analysis
- Quantitative Reverse Transcriptase-Polymerase Chain Reaction (QRT-PCR)
- 5-mC analysis
- QUANTIFICATION AND STATISTICAL ANALYSIS
- DATA AND CODE AVAILABILITY

SUPPLEMENTAL INFORMATION

Supplemental Information can be found online at https://doi.org/10.1016/j.celrep.2019.08.105.

ACKNOWLEDGMENTS

We thank Vasilios Papavasiliou and the McGill Comparative Medicine Animals Resources Centre for assistance with *in vivo* studies, the GCRC Cell Vision Core Facility for assistance with flow cytometry, and Dr. Guy Sauvageau (IRIC, Université de Montréal) for the Ezh2 fl/fl mice. This work was supported by the Terry Fox Research Institute Program Project grant 1048, the Canadian Institutes of Health Research Foundation award FDN-148373, Canadian Epigenetics, Environment and Health Research Consortium Team grant TEC-128089, and a Canada Research Chair in Molecular Oncology 950-231033 (to W.J.M.); the U.S. Department of Defense Congressionally Directed Medical Research Programs Breast Cancer Research Program W81XWH-11-1-0046 (to H.W.S.); the McGill Integrated Cancer Research Training Program of H.W.S. and A.H.); the Systems Biology Program of the Canadian Institutes of Health Research (to A.H.); and the Réseau de Recherche en Cancer of the FRQS (FRQ-34787) and Stand Up To Cancer Canada and the Canadian Cancer Society (SU2C-AACR-DT-1815) (to M.P.).

AUTHOR CONTRIBUTIONS

Conceptualization, W.J.M., A.H., and H.W.S.; Investigation and Analysis, A.H., H.W.S., D.Z., V.S.-G., S.S., J.W., J.P.R., M.S., V.V., L.N.H., K.D., and C.L.; Writing – Original Draft, A.H. and H.W.S.; Writing – Review and Editing, A.H., H.W.S., and W.J.M.; Funding Acquisition, W.J.M., H.W.S., and M.P.; Resources, V.V., E.R.A., T.F.W., L.N.H., and M.P.

DECLARATION OF INTERESTS

The authors declare no competing interests.

Received: February 25, 2019 Revised: July 12, 2019 Accepted: August 29, 2019 Published: October 8, 2019

REFERENCES

Ahuja, N., Easwaran, H., and Baylin, S.B. (2014). Harnessing the potential of epigenetic therapy to target solid tumors. J. Clin. Invest. 124, 56–63.

Andrechek, E.R., Hardy, W.R., Siegel, P.M., Rudnicki, M.A., Cardiff, R.A., and Muller, W.J. (2000). Amplification of the neu/erbB2-oncogene in a mouse model of mammary tumorigenesis. Proc. Natl. Acad. Sci. USA *97*, 3444–3449.

Arnould, L., Gelly, M., Penault-Llorca, F., Benoit, L., Bonnetain, F., Migeon, C., Cabaret, V., Fermeaux, V., Bertheau, P., Garnier, J., et al. (2006). Trastuzumab-based treatment of HER2-positive breast cancer: an antibody-dependent cellular cytotoxicity mechanism? Br. J. Cancer *94*, 259–267.

Barbie, D.A., Tamayo, P., Boehm, J.S., Kim, S.Y., Moody, S.E., Dunn, I.F., Schinzel, A.C., Sandy, P., Meylan, E., Scholl, C., et al. (2009). Systematic RNA interference reveals that oncogenic KRAS-driven cancers require TBK1. Nature 462, 108–112.

Benci, J.L., Xu, B., Qiu, Y., Wu, T.J., Dada, H., Twyman-Saint Victor, C., Cucolo, L., Lee, D.S.M., Pauken, K.E., Huang, A.C., et al. (2016). Tumor Interferon



Signaling Regulates a Multigenic Resistance Program to Immune Checkpoint Blockade. Cell 167, 1540–1554.e12.

Bitler, B.G., Aird, K.M., Garipov, A., Li, H., Amatangelo, M., Kossenkov, A.V., Schultz, D.C., Liu, Q., Shih, IeM., Conejo-Garcia, J.R., et al. (2015). Synthetic lethality by targeting EZH2 methyltransferase activity in ARID1A-mutated cancers. Nat. Med. 21, 231–238.

Chen, E.Y., Tan, C.M., Kou, Y., Duan, Q., Wang, Z., Meirelles, G.V., Clark, N.R., and Ma'ayan, A. (2013). Enrichr: interactive and collaborative HTML5 gene list enrichment analysis tool. BMC Bioinformatics *14*, 128.

Chiappinelli, K.B., Strissel, P.L., Desrichard, A., Li, H., Henke, C., Akman, B., Hein, A., Rote, N.S., Cope, L.M., Snyder, A., et al. (2016a). Inhibiting DNA Methylation Causes an Interferon Response in Cancer via dsRNA Including Endogenous Retroviruses. Cell *164*, 1073.

Chiappinelli, K.B., Zahnow, C.A., Ahuja, N., and Baylin, S.B. (2016b). Combining Epigenetic and Immunotherapy to Combat Cancer. Cancer Res. 76. 1683–1689.

Clynes, R.A., Towers, T.L., Presta, L.G., and Ravetch, J.V. (2000). Inhibitory Fc receptors modulate in vivo cytotoxicity against tumor targets. Nat. Med. 6, 443–446

Dobenecker, M.-W., Kim, J.K., Marcello, J., Fang, T.C., Prinjha, R., Bosselut, R., and Tarakhovsky, A. (2015). Coupling of T cell receptor specificity to natural killer T cell development by bivalent histone H3 methylation. J. Exp. Med. *212*, 297–306.

Finak, G., Bertos, N., Pepin, F., Sadekova, S., Souleimanova, M., Zhao, H., Chen, H., Omeroglu, G., Meterissian, S., Omeroglu, A., et al. (2008). Stromal gene expression predicts clinical outcome in breast cancer. Nat. Med. *14*, 518–527.

Gao, X.-N., Lin, J., Wang, L.-L., and Yu, L. (2009). Demethylating treatment suppresses natural killer cell cytolytic activity. Mol. Immunol. *46*, 2064–2070. Groh, S., and Schotta, G. (2017). Silencing of endogenous retroviruses by heterochromatin. Cell. Mol. Life Sci. *74*, 2055–2065.

Guy, C.T., Cardiff, R.D., and Muller, W.J. (1992). Induction of mammary tumors by expression of polyomavirus middle T oncogene: a transgenic mouse model for metastatic disease. Mol. Cell. Biol. *12*, 954–961.

Holm, K., Grabau, D., Lövgren, K., Aradottir, S., Gruvberger-Saal, S., Howlin, J., Saal, L.H., Ethier, S.P., Bendahl, P.-O., Stål, O., et al. (2012). Global H3K27 trimethylation and EZH2 abundance in breast tumor subtypes. Mol. Oncol. 6, 494–506

Hon, G.C., Hawkins, R.D., Caballero, O.L., Lo, C., Lister, R., Pelizzola, M., Valsesia, A., Ye, Z., Kuan, S., Edsall, L.E., et al. (2012). Global DNA hypomethylation coupled to repressive chromatin domain formation and gene silencing in breast cancer. Genome Res. 22, 246–258.

Huang, S., Li, F., Liu, H., Ye, P., Fan, X., Yuan, X., Wu, Z., Chen, J., Jin, C., Shen, B., et al. (2018a). Structural and functional characterization of MBS301, an afucosylated bispecific anti-HER2 antibody. MAbs 10, 864–875.

Huang, X., Yan, J., Zhang, M., Wang, Y., Chen, Y., Fu, X., Wei, R., Zheng, X.-L., Liu, Z., Zhang, X., et al. (2018b). Targeting Epigenetic Crosstalk as a Therapeutic Strategy for EZH2-Aberrant Solid Tumors. Cell *175*, 186–199.e19.

Ishak, C.A., Marshall, A.E., Passos, D.T., White, C.R., Kim, S.J., Cecchini, M.J., Ferwati, S., MacDonald, W.A., Howlett, C.J., Welch, I.D., et al. (2016). An RB-EZH2 Complex Mediates Silencing of Repetitive DNA Sequences. Mol. Cell 64, 1074–1087.

Italiano, A., Soria, J.-C., Toulmonde, M., Michot, J.-M., Lucchesi, C., Varga, A., Coindre, J.-M., Blakemore, S.J., Clawson, A., Suttle, B., et al. (2018). Tazemetostat, an EZH2 inhibitor, in relapsed or refractory B-cell non-Hodgkin lymphoma and advanced solid tumours: a first-in-human, open-label, phase 1 study. Lancet Oncol. 19. 649–659.

Kauraniemi, P., Hautaniemi, S., Autio, R., Astola, J., Monni, O., Elkahloun, A., and Kallioniemi, A. (2004). Effects of Herceptin treatment on global gene expression patterns in HER2-amplified and nonamplified breast cancer cell lines. Oncogene 23, 1010–1013.

Kim, K.H., Kim, W., Howard, T.P., Vazquez, F., Tsherniak, A., Wu, J.N., Wang, W., Haswell, J.R., Walensky, L.D., Hahn, W.C., et al. (2015). SWI/SNF-mutant

cancers depend on catalytic and non-catalytic activity of EZH2. Nat. Med. 21, 1491–1496.

Kleer, C.G., Cao, Q., Varambally, S., Shen, R., Ota, I., Tomlins, S.A., Ghosh, D., Sewalt, R.G.A.B., Otte, A.P., Hayes, D.F., et al. (2003). EZH2 is a marker of aggressive breast cancer and promotes neoplastic transformation of breast epithelial cells. Proc. Natl. Acad. Sci. USA 100, 11606–11611.

Knutson, S.K., Warholic, N.M., Wigle, T.J., Klaus, C.R., Allain, C.J., Raimondi, A., Porter Scott, M., Chesworth, R., Moyer, M.P., Copeland, R.A., et al. (2013). Durable tumor regression in genetically altered malignant rhabdoid tumors by inhibition of methyltransferase EZH2. Proc. Natl. Acad. Sci. USA *110*, 7922–7927

Lee, H.J., Seo, A.N., Kim, E.J., Jang, M.H., Suh, K.J., Ryu, H.S., Kim, Y.J., Kim, J.H., Im, S.-A., Gong, G., et al. (2014). HER2 heterogeneity affects trastuzumab responses and survival in patients with HER2-positive metastatic breast cancer. Am. J. Clin. Pathol. *142*, 755–766.

Leeb, M., Pasini, D., Novatchkova, M., Jaritz, M., Helin, K., and Wutz, A. (2010). Polycomb complexes act redundantly to repress genomic repeats and genes. Genes Dev. 24, 265–276.

Loibl, S., von Minckwitz, G., Schneeweiss, A., Paepke, S., Lehmann, A., Rezai, M., Zahm, D.M., Sinn, P., Khandan, F., Eidtmann, H., et al. (2014). PIK3CA mutations are associated with lower rates of pathologic complete response to anti-human epidermal growth factor receptor 2 (her2) therapy in primary HER2-overexpressing breast cancer. J. Clin. Oncol. 32, 3212–3220.

Majewski, I.J., Nuciforo, P., Mittempergher, L., Bosma, A.J., Eidtmann, H., Holmes, E., Sotiriou, C., Fumagalli, D., Jimenez, J., Aura, C., et al. (2015). PIK3CA mutations are associated with decreased benefit to neoadjuvant human epidermal growth factor receptor 2-targeted therapies in breast cancer. J. Clin. Oncol. *33*, 1334–1339.

Mayer, E.L., Gropper, A.B., Harris, L., Gold, J.M., Parker, L., Kuter, I., Come, S., Najita, J.S., Guo, H., Winer, E.P., and Burstein, H.J. (2015). Long-term follow-up after preoperative trastuzumab and chemotherapy for HER2-over-expressing breast cancer. Clin. Breast Cancer *15*, 24–30.

Mimura, K., Kono, K., Hanawa, M., Kanzaki, M., Nakao, A., Ooi, A., and Fujii, H. (2005). Trastuzumab-mediated antibody-dependent cellular cytotoxicity against esophageal squamous cell carcinoma. Clin. Cancer Res. *11*, 4898–4904.

Niu, C., Li, M., Zhu, S., Chen, Y., Zhou, L., Xu, D., Li, W., Cui, J., Liu, Y., and Chen, J. (2018). Decitabine Inhibits Gamma Delta T Cell Cytotoxicity by Promoting KIR2DL2/3 Expression. Front. Immunol. 9, 617.

Ochoa, M.C., Minute, L., Rodriguez, I., Garasa, S., Perez-Ruiz, E., Inogés, S., Melero, I., and Berraondo, P. (2017). Antibody-dependent cell cytotoxicity: immunotherapy strategies enhancing effector NK cells. Immunol. Cell Biol. 95, 347–355.

Park, S.E., Park, K., Lee, E., Kim, J.-Y., Ahn, J.S., Im, Y.-H., Lee, C., Jung, H., Cho, S.Y., Park, W.-Y., et al. (2018). Clinical implication of tumor mutational burden in patients with HER2-positive refractory metastatic breast cancer. Oncolmmunology 7, e1466768.

Peng, D., Kryczek, I., Nagarsheth, N., Zhao, L., Wei, S., Wang, W., Sun, Y., Zhao, E., Vatan, L., Szeliga, W., et al. (2015). Epigenetic silencing of TH1-type chemokines shapes turnour immunity and immunotherapy. Nature 527, 249–253.

Rimawi, M.F., Schiff, R., and Osborne, C.K. (2015). Targeting HER2 for the treatment of breast cancer. Annu. Rev. Med. 66, 111–128.

Roulois, D., Loo Yau, H., Singhania, R., Wang, Y., Danesh, A., Shen, S.Y., Han, H., Liang, G., Jones, P.A., Pugh, T.J., et al. (2015). DNA-Demethylating Agents Target Colorectal Cancer Cells by Inducing Viral Mimicry by Endogenous Transcripts. Cell *162*, 961–973.

Scott, M.T., Korfi, K., Saffrey, P., Hopcroft, L.E.M., Kinstrie, R., Pellicano, F., Guenther, C., Gallipoli, P., Cruz, M., Dunn, K., et al. (2016). Epigenetic Reprogramming Sensitizes CML Stem Cells to Combined EZH2 and Tyrosine Kinase Inhibition. Cancer Discov. 6, 1248–1257.

Sharma, S.V., Lee, D.Y., Li, B., Quinlan, M.P., Takahashi, F., Maheswaran, S., McDermott, U., Azizian, N., Zou, L., Fischbach, M.A., et al. (2010). A

chromatin-mediated reversible drug-tolerant state in cancer cell subpopulations. Cell 141, 69-80.

Shen, X., Liu, Y., Hsu, Y.-J., Fujiwara, Y., Kim, J., Mao, X., Yuan, G.-C., and Orkin, S.H. (2008). EZH1 mediates methylation on histone H3 lysine 27 and complements EZH2 in maintaining stem cell identity and executing pluripotency. Mol. Cell 32, 491-502.

Siegel, P.M., Ryan, E.D., Cardiff, R.D., and Muller, W.J. (1999). Elevated expression of activated forms of Neu/ErbB-2 and ErbB-3 are involved in the induction of mammary tumors in transgenic mice: implications for human breast cancer. EMBO J. 18, 2149-2164.

Smith, H.W., Hirukawa, A., Sanguin-Gendreau, V., Nandi, I., Dufour, C.R., Zuo, D., Tandoc, K., Leibovitch, M., Singh, S., Rennhack, J.P., et al. (2019). An ErbB2/c-Src axis links bioenergetics with PRC2 translation to drive epigenetic reprogramming and mammary tumorigenesis. Nat. Commun. 10, 2901.

Snell, L.M., McGaha, T.L., and Brooks, D.G. (2017). Type I Interferon in Chronic Virus Infection and Cancer, Trends Immunol, 38, 542-557.

Spiridon, C.I., Ghetie, M.-A., Uhr, J., Marches, R., Li, J.-L., Shen, G.-L., and Vitetta, E.S. (2002). Targeting multiple Her-2 epitopes with monoclonal antibodies results in improved antigrowth activity of a human breast cancer cell line in vitro and in vivo. Clin. Cancer Res. 8, 1720-1730.

Taplin, M.-E., Hussain, A., Shore, N.D., Bradley, B., Trojer, P., Lebedinsky, C., Senderowicz, A.M., and Antonarakis, E.S. (2018). A phase 1b/2 study of CPI-1205, a small molecule inhibitor of EZH2, combined with enzalutamide (F) or abiraterone/prednisone (A/P) in patients with metastatic castration resistant prostate cancer (mCRPC). J. Clin. Oncol. 36, TPS398-TPS398.

Tong, Q., He, S., Xie, F., Mochizuki, K., Liu, Y., Mochizuki, I., Meng, L., Sun, H., Zhang, Y., Guo, Y., et al. (2014). Ezh2 regulates transcriptional and posttranslational expression of T-bet and promotes Th1 cell responses mediating aplastic anemia in mice. J. Immunol. 192, 5012-5022.

Tumes, D.J., Onodera, A., Suzuki, A., Shinoda, K., Endo, Y., Iwamura, C., Hosokawa, H., Koseki, H., Tokoyoda, K., Suzuki, Y., et al. (2013). The polycomb protein Ezh2 regulates differentiation and plasticity of CD4(+) T helper type 1 and type 2 cells. Immunity 39, 819-832.

Ursini-Siegel, J., Schade, B., Cardiff, R.D., and Muller, W.J. (2007). Insights from transgenic mouse models of ERBB2-induced breast cancer. Nat. Rev. Cancer 7, 389-397.

Ursini-Siegel, J., Hardy, W.R., Zuo, D., Lam, S.H., Sanguin-Gendreau, V., Cardiff, R.D., Pawson, T., and Muller, W.J. (2008). ShcA signalling is essential for tumour progression in mouse models of human breast cancer. EMBO J. 27,

Vance, G.H., Barry, T.S., Bloom, K.J., Fitzgibbons, P.L., Hicks, D.G., Jenkins, R.B., Persons, D.L., Tubbs, R.R., and Hammond, M.E.H.; College of American Pathologists (2009). Genetic heterogeneity in HER2 testing in breast cancer: panel summary and guidelines. Arch. Pathol. Lab. Med. 133, 611–612.

Varadan, V., Gilmore, H., Miskimen, K.L.S., Tuck, D., Parsai, S., Awadallah, A., Krop, I.E., Winer, E.P., Bossuyt, V., Somlo, G., et al. (2016a). Immune Signatures Following Single Dose Trastuzumab Predict Pathologic Response to PreoperativeTrastuzumab and Chemotherapy in HER2-Positive Early Breast Cancer. Clin. Cancer Res. 22, 3249-3259.

Varadan, V., Kamalakaran, S., Gilmore, H., Banerjee, N., Janevski, A., Miskimen, K.L.S., Williams, N., Basavanhalli, A., Madabhushi, A., Lezon-Geyda, K., et al. (2016b). Brief-exposure to preoperative bevacizumab reveals a TGF-β signature predictive of response in HER2-negative breast cancers. Int. J. Cancer 138, 747–757.

Vasanthakumar, A., Xu, D., Lun, A.T., Kueh, A.J., van Gisbergen, K.P., lannarella, N., Li, X., Yu, L., Wang, D., Williams, B.R., et al. (2017). A non-canonical function of Ezh2 preserves immune homeostasis. EMBO Rep. 18, 619-631.

Végran, F., Boidot, R., Coudert, B., Fumoleau, P., Arnould, L., Garnier, J., Causeret, S., Fraise, J., Dembélé, D., and Lizard-Nacol, S. (2009). Gene expression profile and response to trastuzumab-docetaxel-based treatment in breast carcinoma. Br. J. Cancer 101, 1357-1364.

Walter, M., Teissandier, A., Pérez-Palacios, R., and Bourc'his, D. (2016). An epigenetic switch ensures transposon repression upon dynamic loss of DNA methylation in embryonic stem cells. eLife 5, R87.

Wang, X., Wang, J., Yu, Y., Ma, T., Chen, P., Zhou, B., and Tao, R. (2017). Decitabine inhibits T cell proliferation via a novel TET2-dependent mechanism and exerts potent protective effect in mouse auto- and allo-immunity models. Oncotarget 8, 56802-56815.

Wilken, J.A., and Maihle, N.J. (2010). Primary trastuzumab resistance: new tricks for an old drug. Ann. N Y Acad. Sci. 1210, 53-65.

Yadav, K., Shimasaki, N., Ow, S.G.W., Wong, A.L.A., Lim, J.S.J., Koe, P., Koh, L.P., Tan, L.K., Goh, B.C., Campana, D., and Lee, S.-C. (2019). Tumor pathological and immunological changes in HER2+ metastatic breast cancer (MBC) following trastuzumab combined with expanded and activated autologous natural killer (NK) cell infusion. J. Clin. Oncol. 37 (15_suppl).

Yang, X., Zhang, X., Fu, M.L., Weichselbaum, R.R., Gajewski, T.F., Guo, Y., and Fu, Y.-X. (2014). Targeting the tumor microenvironment with interferon-β bridges innate and adaptive immune responses. Cancer Cell 25, 37-48.

Yin, J., Leavenworth, J.W., Li, Y., Luo, Q., Xie, H., Liu, X., Huang, S., Yan, H., Fu, Z., Zhang, L.Y., et al. (2015). Ezh2 regulates differentiation and function of natural killer cells through histone methyltransferase activity. Proc. Natl. Acad. Sci. USA 112, 15988-15993.

Yoneyama, M., Onomoto, K., Jogi, M., Akaboshi, T., and Fujita, T. (2015). Viral RNA detection by RIG-I-like receptors. Curr. Opin. Immunol. 32, 48-53.

Zhang, H., Wang, Q., Montone, K.T., Peavey, J.E., Drebin, J.A., Greene, M.I., and Murali, R. (1999). Shared antigenic epitopes and pathobiological functions of anti-p185(her2/neu) monoclonal antibodies. Exp. Mol. Pathol. 67, 15-25.

Zhao, E., Maj, T., Kryczek, I., Li, W., Wu, K., Zhao, L., Wei, S., Crespo, J., Wan, S., Vatan, L., et al. (2016). Cancer mediates effector T cell dysfunction by targeting microRNAs and EZH2 via glycolysis restriction. Nat. Immunol. 17,



STAR***METHODS**

KEY RESOURCES TABLE

| REAGENT or RESOURCE | SOURCE | IDENTIFIER |
|--|---|---|
| Antibodies | | |
| H3K27me ³ (C36B11) | Cell Signaling | Cat# 9733; RRID: AB_11220433 |
| H3K27me ³ | Millipore | Cat# 07-449; RRID: AB_310624 |
| Normal rabbit IgG | Cell Signaling | Cat# 2729; RRID: AB_1031062 |
| Ezh2 (D2C9) XP | Cell Signaling | Cat# 5246; RRID: AB_10694683 |
| ErbB2/c-Neu (AB3) | Millipore | Cat# OP15L; RRID: AB_2099415 |
| α-Tubulin | Cell Signaling | Cat# 2144; RRID: AB_2210548 |
| 3-Actin | Sigma-Adrich | Cat# A5316; RRID: AB_476743 |
| Histone H3 | Cell Signaling | Cat# 14269; RRID: AB_2756816 |
| STAT1 | Cell Signaling | Cat# 9176; RRID: AB_2240087 |
| P-STAT1 Tyr701 | Cell Signaling | Cat# 9167; RRID: AB_561284 |
| MAVS | Cell Signaling | Cat# 4983; RRID: AB_823566 |
| GAPDH | Novus | Cat# NB100-56875; RRID: AB_838305 |
| Akt | Cell Signaling | Cat# 2920; RRID: AB_1147620 |
| P-Akt Ser473 | Cell Signaling | Cat# 4060; RRID: AB_2315049 |
| ERK1/2 | Cell Signaling | Cat# 9102; RRID: AB_330744 |
| P-ERK1/2 Thr202/Tyr204 | Cell Signaling | Cat# 9101; RRID: AB_331646 |
| Human Type 1 IFN neutralizing antibody mixture | PBL Assay Science | Cat# 39000-1 |
| Drosophila H2Av | Active Motif | Cat# 61686; RRID: AB_2737370 |
| CD3- efluor450 | Thermo Fisher Scientific | Cat# 48-0032-80; RRID: AB_1272229 |
| CD4- efluor780 | Thermo Fisher Scientific | Cat# 47-0042-82; RRID: AB_1272183 |
| CD8-V500 | BD Biosciences | Cat# 560776; RRID: AB_1937317 |
| CD11c-PeCy5.5 | BD Biosciences | Cat# 560584; RRID: AB_1727422 |
| CD11b- efluor450 | Thermo Fisher Scientific | Cat# 48-0112-80; RRID: AB_1582237 |
| CD19-APC | Thermo Fisher Scientific | Cat# 17-0193-80; RRID: AB_1659678 |
| CD45-PE | BD PharMingen | Cat# 553081; RRID: AB_394611 |
| F4/80- PeCy7 | Thermo Fisher Scientific | Cat# 25-4801-82; RRID: AB_469653 |
| Gr1-FITC | Thermo Fisher Scientific | Cat# 11-5931-82; RRID: AB_465314 |
| CD24-Pacific blue, clone m1/69 | BioLegend | Cat# 101814; RRID: AB_439716 |
| CD29-PeCy7 | Thermo Fisher Scientific | Cat# 25-0291-82; RRID: AB_1234962 |
| CD49b- PeCy7 | Thermo Fisher Scientific | Cat# 25-5971-81; RRID: AB_469666 |
| Ter119-PE | BioLegend | Cat# 116207; RRID: AB_313708 |
| CD31-PE | BioLegend | Cat# 102507; RRID: AB_312914 |
| pan-Cytokeratin | Roche | Cat# 760-2135; RRID: AB_2810237 |
| Alexa Fluor 488 Donkey anti-Rabbit Fisher Scientific,; A31571; - Fisher Scientific, | Thermo Fisher Scientific | Cat# A21206; RRID: AB_2535792 |
| Alexa Fluor 555 Donkey anti-Rabbit | Thermo Fisher Scientific | Cat# A31572; RRID: AB_162543 |
| Alexa Fluor 488 Donkey anti-Mouse | Thermo Fisher Scientific | Cat# A21202; RRID: AB_141607 |
| Alexa Fluor 647 Goat anti-Guinea pig | Thermo Fisher Scientific | Cat# A21450; RRID: AB_2735091 |
| RDye 800CW Donkey anti-rabbit | LI-COR Biosciences | Cat# 925-32213; RRID: AB_2715510 |
| RDye680CW Donkey anti-mouse | LI-COR Biosciences | Cat# 926-68072; RRID: AB_10953628 |
| ErbB2 mAb 7.16.4 | Produced from Hybridoma (ATCC) and also purchased from BioXcell | ATCC Cat# HB-10493; RRID: CVCL_X742 |
| | | BioXCell: Cat# BE0277; RRID: AB_2687800 |
| ERBB2 mAb 4D5 | Genentech | N/A |

(Continued on next page)

| Continued | | |
|--|--|--------------------------------|
| REAGENT or RESOURCE | SOURCE | IDENTIFIER |
| Pab101 (anti-SV40 Large-T antigen) | Produced from Hybridoma (ATCC) | Cat# TIB-117; RRID: CVCL_4609 |
| Mouse IgG1 isotype control | Sigma | Cat# M5284; RRID: AB_1163685 |
| Bacterial and Virus Strains | | |
| Ad5CMVcytoLacZ | U. of Iowa Carver College of Medicine Viral Vector Core | Cat# VVC-U of Iowa-3554 |
| Ad5CMVCre | U. of Iowa Carver College of Medicine Viral Vector Core | Cat# VVC-U of Iowa-5 |
| Biological Samples | | |
| Fetal Bovine Serum | Wisent Inc. | Cat# 080-150 |
| Bovine Pituitary Extract | Hammond Cell Tech | Cat# 1078-NZ |
| Drosophila Chromatin | Active Motif | Cat# 53083 |
| Chemicals, Peptides, and Recombinant Protein | s | |
| Recombinant human EGF | Wisent | Cat# 511-110-UM |
| Recombinant human insulin | Wisent | Cat# 511-016-UG |
| Hydrocortisone | Sigma | Cat# H4001 |
| Lipofectamine 3000 Transfection Reagent | Thermo Fisher | Cat# L3000075 |
| Polybrene | Sigma | Cat# 107689 |
| Puromycin | BioShop | Cat# PUR333 |
| GSK126 | Mercachem | Custom synthesis |
| EPZ-6438 | MedChem Express | Cat# HY-13803 |
| 5-aza-2-deoxycytidine | Sigma | Cat# A3656 |
| Sulfobutylether-β-cyclodextrin (Captisol) | MedChem Express | Cat# HY-17031 |
| MuMLV Reverse Transcriptase | New England Biolabs | Cat# M0253 |
| Murine RNase inhibitor | New England Biolabs | Cat# M0314 |
| Light Cycler 480 SYBR Green I Master Mix | Roche | Cat# 04887352001 |
| Magna ChIP Protein A/G beads | Millipore | Cat# 16-663 |
| Collagenase B | Roche | Cat# 11088831001 |
| Dispase II | Roche | Cat# D4693 |
| Liberase | Roche | Cat# LIBDL-RO |
| DNase | Roche | Cat# 4942078001 |
| DAPI (4',6-Diamidino-2-Phenylindole, Dihydrochloride) | Thermo Fisher | Cat# D1306 |
| ImmuMount | Thermo Scientific | Cat# 9990412 |
| Critical Commercial Assays | | |
| RNEasy mini kit | QIAGEN | Cat# 74106 |
| QiaQuick PCR purification kit | QIAGEN | Cat# 28106 |
| ImmPRESS HRP Anti-Mouse Polymer Detection Kit | Vector Elite | Cat# MP-7402; RRID: AB_2336528 |
| ImmPRESS HRP Anti-Rabbit Polymer Detection Kit | Vector Elite | Cat# MP-7401; RRID: AB_2336529 |
| CyQuant Cell Proliferation Assay kit | Thermo Fisher | Cat# C7026 |
| Methylated DNA Quantification Kit | Abcam | Cat# ab233486 |
| Mouse IFNγ ELISA kit | RandD Systems | Cat# MIF00 |
| Human IFNβ ELISA kit | PBL Assay Science | Cat# 41410 |
| Episeeker Histone Extraction Kit | Abcam | Cat# ab113476 |
| Deposited Data | | |
| Gene Expression Microarray data | This paper | GEO: GSE136157 |
| Gene Expression RNA-Seq data | This paper | GEO: GSE136300 |

(Continued on next page)



| Continued | | |
|---|--|---|
| REAGENT or RESOURCE | SOURCE | IDENTIFIER |
| H3K27me ³ ChIP-Seq data | This paper | GEO: GSE136205 |
| Experimental Models: Cell Lines | | |
| MMTV-NIC murine mammary tumor cell lines | This paper | N/A |
| MMTV-NDL2-5 murine mammary tumor cell lines | This paper | N/A |
| 293T cells | ATCC | Cat# CRL-3216; RRID: CVCL_0063 |
| SkBr3 cells | ATCC | Cat# HTB-30; RRID: CVCL_0033 |
| HCC1954 cells | ATCC | Cat# CRL-2338; RRID: CVCL_1259 |
| HCC202 cells | ATCC | Cat# CRL-2316; RRID: CVCL_2062 |
| UACC-893 cells | ATCC | Cat# CRL-1902; RRID: CVCL_1782 |
| MCF7 cells | ATCC | Cat# HTB-22; RRID: CVCL_0031 |
| T47D cells | ATCC | Cat# HTB-133; RRID: CVCL_0553 |
| HCC1500 cells | ATCC | Cat# CRL-2329; RRID: CVCL_1254 |
| MDA-MB-175-VII cells | ATCC | Cat# HTB-25; RRID: CVCL_1400 |
| MDA-MB-231 cells | ATCC | Cat# HTB-26; RRID: CVCL_0062 |
| BT549 cells | ATCC | Cat# HTB-122; RRID: CVCL_1092 |
| Hs578t cells | ATCC | Cat# HTB-126; RRID: CVCL_0332 |
| Experimental Models: Organisms/Strains | | |
| Mouse: Ezh2L/L (Ezh2 conditional allele) B6;129S1-Ezh2tm2Sho/J – backcrossed onto FVB/N for six generations prior to use. | Dr. Stuart Orkin, Shen et al., 2008, and The Jackson Laboratory | JAX mice stock# 022616; RRID: IMSR_JAX:022616 |
| Mouse: JAX mice NOD.Cg- Prkdc ^{scid} ll2rg ^{tm1Wjl} /SzJ (NOD/SCID/ gamma) | Charles River | JAX mice stock# 005557; RRID: IMSR_JAX:005557 |
| Mouse: MMTV-NIC (NeuNDL2-5-IRES-Cre) (FVB-Tg(MMTV-Erbb2*,-cre)1Mul/J) | Ursini-Siegel et al., 2008 and The Jackson Laboratory | JAX mice stock# 032576; RRID: IMSR_JAX:032576 |
| Mouse: MMTV-NeuNDL2-5 | Siegel et al., 1999 | N/A |
| Mouse: FVB/N | The Jackson Laboratory | JAX mice stock# 001800; RRID: IMSR_JAX:001800 |
| Mouse: MMTV-Neu N202 (FVB/N- Tg(MMTVneu)202Mul/J) | Guy et al., 1992 and The Jackson Laboratory | JAX mice stock# 002376; RRID: IMSR_JAX:002376 |
| Mouse: MMTV-Cre | Andrechek et al., 2000 | N/A |
| Recombinant DNA | | |
| Plasmid: pMD2.G | Addgene – Dr. Didier Trono | Cat#12259; RRID: Addgene_12259 |
| Plasmid: psPax2 | Addgene – Dr. Didier Trono | Cat#12260; RRID: Addgene_12260 |
| Plasmid: pLKO.1shMavs | Genetic Perturbation Service, Goodman Cancer Research Centre, McGill University. | The RNAi Consortium (TRC) #TRCN0000124769 |
| Oligonucleotides | | |
| | | Refer to Table S2. |
| Software and Algorithms | | |
| Prism version 5.0 | GraphPad | http://www.graphpad.com |
| Excel 2010 | Microsoft | https://products.office.com/ previous-versions/microsoft-excel-2010 |
| Expression Console | Affymetrix/Thermo Fisher | https://www.thermofisher.com/us/en/home/life-science/microarray-analysis/microarray-analysis-instruments-software-services/microarray-analysis-software/affymetrix-transcriptome-analysis-console-software.html |
| | | (0 |

(Continued on next page)

| Continued | | |
|--------------------------------------|------------------------------------|---|
| REAGENT or RESOURCE | SOURCE | IDENTIFIER |
| Transcriptome Analysis Console (TAC) | Affymetrix/Thermo Fisher | https://www.thermofisher.com/us/en/home/life-science/microarray-analysis/microarray-analysis-instruments-software-services/microarray-analysis-software/affymetrix-transcriptome-analysis-console-software.html |
| Ingenuity Pathway Analysis (IPA) | QIAGEN | https://www.qiagenbioinformatics.com/ products/ingenuity-pathway-analysis/# |
| EnrichR | http://amp.pharm.mssm.edu/Enrichr/ | Chen et al., 2013 |
| LiCOR Odyssey v3.0 | LiCOR Biosciences | https://www.licor.com/bio/ |
| Light Cycler 480 Analysis | Roche | Cat# 04994884001 |
| HALO | Indica Labs | http://www.indicalab.com/halo/ |

LEAD CONTACT AND MATERIALS AVAILABILITY

This study did not generate new unique reagents. Further information and requests for resources and reagents should be directed to and will be fulfilled by the Lead Contact, William J. Muller (william.muller@mcgill.ca)

EXPERIMENTAL MODEL AND SUBJECT DETAILS

Animal Models

All experiments involving mice were carried out under protocols approved by the McGill University Animal Care Committee (UACC) and guidelines stipulated by the Canadian Council on Animal Care (CCAC). MMTV-NIC, MMTV-NeuNDL2.5, and *Ezh2* conditional knockout mice were described previously (Shen et al., 2008; Siegel et al., 1999; Ursini-Siegel et al., 2007). Cell lines derived from the MMTV-NIC tumor model were injected into the cleared inguinal mammary fat pads of female immunocompetent N202/MMTV-Cre mice^{57,58} (5x10⁵ tumor cells per mouse). Patient-derived xenografts (PDX) were implanted into female NOD/SCID/gamma (NSG) immunocompromised mice (Charles River Laboratories).

Mice were randomly assigned to treatment groups and monitored for tumor growth by twice-weekly palpation. Treatments began once tumors had reached a size of 5 mm x 5 mm (approximately 65 mm³). GSK126 (custom synthesis by MercaChem) in 20% Sulfobutylether-β-cyclodextrin (Captisol - Medchem Express) was administered at 300 mg/kg three times per week by intraperitoneal injection. 7.16.4 mAb was administered in doses of 100 μg via intraperitoneal injection, 2 times per week. Control mice received equivalent volumes of vehicle (20% Captisol) and an isotype-matched control antibody (clone Pab101, versus SV40 Large-T antigen) via intraperitoneal injection, following the same schedule. Hybridomas were purchased from ATCC and antibodies produced by GenScript. Mice were weighed twice weekly and doses were adjusted according to bodyweight. Tumor growth was measured by twice-weekly caliper measurements. Drug administration, data collection and data analysis were performed by separate individuals who were blinded with respect to the treatment group of each mouse.

Human Subjects

PDX GCRC1991 was established from a tumor sample from a 42 year-old female patient who underwent surgical excision of ERBB2+ invasive ductal adenocarcinoma at the Jewish General Hospital, McGill University, Montreal, QC, with informed consent under a protocol approved by the Research Ethics Office of the Faculty of Medicine, McGill University.

Matched tumor tissue samples collected pre- and post- Trastuzumab treatment are described in detail elsewhere (Varadan et al., 2016a). Briefly, samples were collected from stage II-III ERBB2+ breast cancer patients enrolled in phase II neoadjuvant trials (03-311, NCT00148668; and BrUOG 211B, NCT00617942). Informed consent was received from all patients prior to biopsy, after which the patient then received a loading dose of trastuzumab (8mg/kg) and repeat biopsies were collected 14 days later. Pathologic clinical response (pCR) was scored by institutional pathologists during the completion of preoperative therapy, with pCR defined as the absence of residual invasive disease in both the breast and any sampled axillary nodes. Normalized RNA-Seq gene expression profiles (log2-FPKM) were obtained for breast cancer biopsy samples in the BrUOG 211B (NCT00617942) clinical trial cohort as previously described (Varadan et al., 2016b). Patient response to preoperative Trastuzumab and chemotherapy was assessed using the Residual Cancer Burden methodology as previously described (Varadan et al., 2016a). pCR (RCB0) and RCB1 were designated as responders, while RCB2 and RCB3 were designated as non-responders. The EZH2 and H3K27me³ levels were assessed by immunofluorescence in core biopsies of breast tumor from the same patients.



Primary Cell Cultures and Cell Lines

This study used primary cultures and cell lines derived from mammary tumors of female MMTV-NIC and MMTV-NDL2-5 transgenic mice. Tumors were processed with a McIlwain tissue chopper (Mickle Laboratory Engineering), dissociated in collagenase B/Dispase II (Roche) for 1 h at 37C, washed three times with PBS/1mM EDTA and plated in Complete Media (DMEM supplemented with 5% FBS, EGF (5 ng/ml), Hydrocortisone (1 μg/ml), Insulin (5 μg/ml) and Bovine Pituitary Extract (BPE) (35 μg/ml)). Cells were grown in a humidified, 5% CO2, 37°C incubator in Complete Media. The genotype of murine cell lines was authenticated by PCR on genomic DNA to detect the presence of the MMTV-NIC or MMTV-NDL transgenes and the presence of wild-type and LoxP-flanked conditional alleles and also by immunoblotting to detect the expression of ErbB2, Cre recombinase and Ezh2 proteins.

Human cell lines

Human breast cancer cell lines (see Key Resource Table) and 293T cells (for lentivirus production) were purchased from ATCC, used at early passage and were not authenticated.

METHOD DETAILS

In vitro experiments

GSK126 and EPZ-6438 were reconstituted in DMSO and administered for 7 days, with replenishment on days 3 and 5. Cells were seeded into 96 well plates for proliferation assays or histones were extracted for immunoblotting analysis on day 5. For in vitro ablation of Ezh2, NeuNDL2.5 cells were infected with adenoviruses encoding Cre Recombinase or Lac Z (Gene Transfer Vector Core, lowa State University) and used at 72 h post-infection. 5-aza-2'-deoxycytidine (Sigma) was used at 100nM for 72 h prior to assays. Global DNA methylation status was assessed using a colorimetric Methylated DNA Quantification Kit (Abcam). Human Type 1 IFN neutralizing antibody mixture (PBL Assay Science) was administered 24 and 72 h after plating cells (1:50, as per manufacturer's instructions). Anti-ErbB2 mAbs 4D5 (non-humanized version of Trastuzumab - a gift of Genentech, a member of the Roche group) and 7.16.4 (BioXCell, BE0277) were administered to cultured cells at the concentrations indicated in the figures for 96h. Cell proliferation was analyzed by using the CyQuant assay (Thermo Fisher, C7026), which is a fluorometric assay measuring nucleic acid content as a proxy of cell number, or by phase-contrast based image analysis of cell confluency using the Incucyte Zoom instrument (Essen Biosciences), with images taken at defined time points using a 10x objective and analysis using the associated software according to the manufacturer's protocols.

Lentiviral Production and Transduction

Lentiviruses bearing shRNA against MAVS were produced in 293T cells (ATCC) co-transfected with the vectors pMD2.G and psPAX2, gifts from Dr. Didier Trono (Addgene plasmids #12259 and #12260). Lipofectamine 3000 (Invitrogen, L3000075) was used for transfection according to the manufacturer's instructions and virus-containing media was harvested and filtered through a 0.45 μm filter at 24 and 48h post-transfection. MMTV-NIC cells were transduced in the presence of 10 μg/ml polybrene (Sigma, 107689). Transduced cell lines were selected and maintained in Complete Media with 2 μg/ml puromycin (BioShop, PUR333).

Adenovirus Infection

Adenoviruses bearing Cre recombinase or LacZ were purchased from the Viral Vector Core Facility of the University of Iowa Carver College of Medicine. MMTV-NDL2-5 cells were infected at a MOI of 25 overnight in complete media with reduced serum (1% FBS), with media replenished the following morning.

Transcriptional Profiling - Microarray

Affymetrix GeneChip Mouse Gene 2.0 ST arrays were used, according to the manufacturer's protocols, to analyze gene expression in 2 independent NIC cell lines treated with GSK126 or DMSO for 72 h prior to RNA extraction. Total RNA was extracted using the RNEasy kit (QIAGEN) and quantified using a NanoDrop Spectrophotometer ND-1000 (NanoDrop Technologies, Inc.) RNA integrity was assessed using a Bioanalyzer 2100 (Aglient Technologies).

Transcriptional Profiling - RNA Sequencing

RNA from 2 independent samples per condition were isolated using the RNeasy kit (QIAGEN). RNA-seq was peformed by Novogene (Beijing, China). Briefly, 4ug of total RNA was used for sequencing library preparation using either the NEBNext UltraTM RNA Library Prep Kit for Illumina (NEB) following manufacturer's instructions for mRNA sequencing, or the Ribo-Zero TM Magnetic Kit (Illumina) 250-300 base pair insert stand specific library with rRNA removal. PCR products were purified using AMPure XP system (Beckman Coulter), and library quality was assessed on the Agilent Bioanalyzer 2100 system. Samples were sequenced on an Illumina HiSeq platform (paired end, 150 base pairs).

For analysis of coding region gene expression on average, 40 million reads were obtained per sample. For analysis of non-coding regions, on average 100 million reads were obtained per sample. Raw read of fastq format were then processed through Novogene in-house perl scripts to obtain clean reads, by removing reads containing adapters, reads containing poly-N and low quality reads from raw data. Index of the mm10 mouse or hg19 human genome was built using Bowtie v2.2.3, and paired-end clean reads were



aligned to the reference genome using TopHat v2.0.12. HTSeq v0.6.1 was used to count the reads numbers mapped to each gene. FPKM (fragments per kilobase of transcript per million mapped reads) of each gene was calculated based on the length of the gene and reads count mapped to this gene. Differential expression analysis was performed using the DESeq R package (1.18.0). The p values were adjusted using Benjamini and Hochberg's method. Genes with an adjusted p value < 0.05 were considered as differentially expressed.

Chromatin Immunoprecipitation (ChIP)

5 μg of anti-H3K27me³ (Millipore) or Normal rabbit IgG (Cell Signaling) was immobilized overnight at 4°C on 20 μL of Magna ChIP Protein A+G magnetic beads (Millipore) diluted in 250 μL of PBS + 0.5% BSA and then washed 3 times with PBS + 0.5% BSA. Approximately 3 × 10⁷ NIC cells were fixed with a 1% final concentration of formaldehyde for 5 min at room temperature and then lysed and sonicated. Equal amounts of chromatin were diluted in 2.5X ChIP dilution buffer (EDTA 2 mM, NaCl 100 mM, Tris 20 mM, Triton 0.5%) + 100 μL of PBS+0.5% BSA and added to the antibody-bound beads and left to rotate overnight at 4°C. Next, beads were washed 3 times for 3 min at 4°C with 1 mL LiCl buffer (Tris 100mM, LiCl 500 mM, Na-deoxycholate 1%) then once with 1 mL TE buffer. DNA was eluted with 150 μL of elution buffer (0.1M NaHCO₃, 0.1% SDS) overnight at 65°C. Precipitated DNA was purified using a QIAquick PCR purification kit (QIAGEN) and eluted in 60 µL of elution buffer. ChIP normalization was used to reduce the effects of technical variation and sample processing bias, as outlined by manufacturer's instructions (ChIP Spike-in Normalization Strategy, Active Motif).

Analysis of Gene Expression Data

Ingenuity pathway analysis (IPA) of microarray target genes analysis of target genes was done using Ingenuity Pathway Analysis Software (Ingenuity Systems). Canonical pathway analysis identified significant pathways from the IPA library using Fisher's exact test to calculate p values. Reactome pathway analysis were performed using the EnrichR online tool (http://amp.pharm.mssm.edu/Enrichr/) (Chen et al., 2013).

CHIP-Seq Analysis

After isolation of the DNA, it was sequenced using AAA base pair Paired end sequencing and reported as .fastq files. Data were assayed for quality through the use of FASTQC and processed using trimmomatic1. Drosophila and mouse DNA was aligned to the BDGP6 and mm10 reference genomes respectively through the use of BWA2. As previously described the mouse data were normalized to remove background noise through the removal of random reads through the use of the Drosophila data. After the removal of PCR bias and other artifacts through the use of SAMtools³ and PICARDtools using default parameters, broad peaks were called through the use of MACS2 with default parameters.

RNA-Seq Analysis

Processing of RNA-Seq data were completed using a standard Tuxedo analysis pipeline. Data were assessed for quality control through the use of FASTQC followed by Trimmomatic. The processed .fastq file was aligned to the mm10 reference genome through the use of bowtie2. After standard processing the normalized gene expression table was analyzed through the use of single sample gene set enrichment analysis on genepattern.

Viral Defense Gene Expression Signature

The per sample enrichment indices for the viral defense gene expression signature (Chiappinelli et al., 2016a)and the Reactome IFN Signature were calculated on a per-sample basis using Single-Sample Gene Set Enrichment Analysis (ssGSEA) (Barbie et al., 2009). These indices were compared in HER2+ patient tumor samples obtained prior to treatment (Base) and 14 days after (Post) a loading dose of Trastuzumab within each response category using a One-Tailed Student T-Test. Similar analyses were conducted using the H3K27me³-positive Intensities. Correlations of the percentage of H3K27me³-positive versus EZH2-Positive cells, as well as H3K27me³-positive cells and the Reactome IFN signature indices was assessed using Pearson Correlation measure.

Retrotransposon expression analysis

After demultiplexing, reads for both human and mouse samples were processed using SAMtools (v1.4) and aligned using Hisat2 (v2.0.4) (PMID: 25751142) with default parameters. The coordinates and gene annotations used were based on the human (hg38/ GRCh38) and mouse (mm10/GRCm38) reference genome builds. Annotations for repeat elements were obtained from Repeat-Masker (open-4.0.5). Quantitation of reads mapping to annotated repeat elements was performed using the Python module Pysam (https://github.com/pysam-developers/pysam). Expression was then RPKM normalized. For inclusion in downstream analysis, retrotransposable elements were required to have 10 mapped reads in at least one of the samples analyzed.



ELISA

The Enzyme-linked immunosorbent assay (ELISA) was performed using the eBioscience mouse IFN_γ kit (MIF00, RandD Systems) or human IFN \(\text{kit} \) (PBL Assay Science). The protocol was followed as described in the technical manuals from the company, with a few exceptions: protein lysates from samples were used at 50 µg total protein concentration and the sample. Incubation was performed overnight at 4°C.

Flow cytometry

Mammary glands or tumors were excised and finely chopped using the McIlwain Tissue Chopper and dissociated in DMEM (Wisent) containing 320 μL Liberase (160 μg/mL, Roche) and 200 μL of DNase (200mg/mL) for 45 min at 37°C, with constant agitation. The cell suspensions were incubated for 3 min with Lysis Buffer (NH4Cl solution) and two times in PBS with centrifugation at 3500RPM for 5 min at room temperature. For flow cytometry analysis cell suspensions were resuspended in PBS and filtered through 100 µm mesh and resuspended in 500 µL FACS Buffer (PBS with 5% FBS). Dissociated cell samples were incubated with fluorescently conjugated antibodies for 30 min at 4°C and washed in PBS. Samples were run using the BD FACS Cantoll and data from 100,000-250,000 events were collected from samples. Data were analyzed using FloJo Software. The following antibodies were used; CD3- efluor450 (1:100, 48-0032-82 eBioscience), CD4- efluor780 (1:100, 47-0042-82 eBioscience), CD8-V500 (1:200 560776 BD PharMingen), CD11c-PeCy5.5 (1:100, 560584 eBioscience), CD11b- efluor450 (1:100, 48-0112-80 BD PharMingen), CD19-APC (1:100, 17-0193-80 eBioscience), CD45-PE (1:300, 17-0193-80 BD PharMingen)

F4/80- PeCy7 (1:100, 25-4801-82 eBioscience), Gr1-FITC (1:100, 11-5931-82 eBioscience), CD24-Pacific blue (1:300, 101814 clone m1/69 BioLegend), CD29-PeCy7 (1:300, 25-0291-82 eBioscience), CD49b- PeCy7 (1:100, 25-5971-81 eBioscience), Ter119-PE (1:300, 116207 BioLegend), and CD31-PE (1:300, 102507 BioLegend).

Protein Extraction and Immunoblotting

Freshly excised tumor tissue was immediately flash-frozen in liquid nitrogen, crushed with a mortar and pestle under liquid nitrogen, allowed to thaw briefly and then lysed in ice-cold RIPA buffer (Tris-HCl 50 mM, pH 7.4, sodium chloride 150 mM, Nonidet P-40 1%, sodium deoxycholate 1%, SDS 0.1%, 2 mM EDTA, 0.5 mM AEBSF, 25 mM β-glycerophosphate, 1 mM sodium orthovanadate, and 10 mM sodium fluoride). Cultured cells were lysed on ice in RIPA buffer. For immunoblotting of histones, the Episeeker Histone Extraction Kit (Abcam) was used to extract histones according to the manufacturer's instructions. Protein concentrations were determined by Bradford assay and 30 µg of total protein or 5ug of extracted histones were analyzed by immunoblot as previously described¹⁹. A Li-COR Odyssey system (Li-COR Biosciences) was used for fluorescent immunoblotting and quantification was performed using associated software. The following antibodies were used: H3K27me3 (C36B11 - Cell Signaling, 1/1000, Cat# 9733); Ezh2 (D2C9) XP Cell Signaling Cat# 5246; β-Actin (Sigma-Aldrich, 1/2500, Cat# A5316), Histone H3 (Cell Signaling, 1/1000, Cat# 14269); STAT1 (Cell Signaling, 1/1000, Cat# 9176); P-STAT1 Tyr701 (Cell Signaling, 1/500, Cat# 9167); MAVS (Cell Signaling, 1/500, Cat# 4983); GAPDH (Novus, 1/2000, Cat# NB100-56875); pan-Akt (Cell Signaling, 1/1000, Cat# 2920); P-Akt Ser473 (Cell Signaling, 1/1000, Cat# 4060); ERK1/2 (Cell Signaling, 1/1000, Cat# 9102); P-ERK1/2 Thr202/Tyr204 (Cell Signaling, 1/1000, Cat# 9101).

Immunofluorescence and analysis

Frozen sections of primary tumor core biopsy material from cohorts of HER2+ patients (described above) were fixed in 2% formalin and blocked with 10% Power Block (BioGenex, HK083) in PBS for 10 min at room temperature. Sections were incubated with primary antibodies at 4°C overnight and with secondary antibodies for one h at room temperature, followed by DAPI (4',6-Diamidino-2-Phenylindole, Dihydrochloride, ThermoFisher, D1306) for 15 min, washed three times in PBS and mounted in ImmuMount (Thermo Scientific, 9990412). Primary antibodies used were: H3K27me3 (C36B11) - Cell Signaling, 9733, 1/100; Ezh2 (D2C9) XP - Cell Signaling, 5246, 1/500; ErbB2/c-Neu (AB3) - Calbiochem, OP15, 1/100; pan-Cytokeratin - Ventana, 760-2135, undiluted. Secondary antibodies were Alexa Fluor 488 Donkey anti-Rabbit - Fisher Scientific, A21206; Alexa Fluor 555 Donkey anti-Rabbit - Fisher Scientific, A31572; Alexa Fluor 488 Donkey anti-Mouse - Fisher Scientific, A21202; A31571; Alexa Fluor 647 Goat anti-Guinea pig - Fisher Scientific, A21450. All fluorescent secondary antibodies were used at a dilution of 1/1000. Images were acquired using a Zeiss Axio Scan.Z1 slide scanner running ZEN software and analyzed using the HALO Highflex FL module algorithm (Indica Labs) to quantify the EZH2 and H3K27me³ signals specifically in the nuclei of pan-Cytokeratin-positive tumor cells, excluding the stroma. Average signal intensities were calculated for each sample, and cells were also binned by fluorescence intensity ranging from 0 (no signal), 1 (weak signal), 2 (moderate signal) to 3+ (strong signal). Samples were divided into responders and non-responders based on clinical criteria described above.

Quantitative Reverse Transcriptase-Polymerase Chain Reaction (QRT-PCR)

Total RNA was extracted from flash frozen mammary tumors using an RNeasy Mini Kit. cDNA was prepared by reverse transcribing the isolated RNA using M-Mulv Reverse Transcriptase, Oligo-dT(23VN) and murine RNase inhibitor. Real-time quantitative PCR was performed using LightCycler 480 SYBR Green I MasterMix and LightCycler 480 instrument (Roche) and analyzed using associated software.



5-mC analysis

5-mC was quantified in genomic DNA isolated from cell lines using a DNEasy mini kit (QIAGEN, 69504). A modified ELISA with color-imetric detection performed on immobilized genomic DNA in a 96wp format (Abcam, ab233486) was used according to the manufacturer's instructions. The manufacturer's data show that results obtained using this assay correlate closely with detection of 5-methylcytosine by LC/MS.

QUANTIFICATION AND STATISTICAL ANALYSIS

Information on group sizes and statistical tests are in the figure legends. In general, unpaired two-tailed Student's t tests were performed in GraphPad Prism or Microsoft Excel software unless otherwise specified. One-way ANOVA with Tukey's post hoc test for multiple comparisons and Kaplan-Meier analysis with logrank tests (Mantel-Haenszel) were performed using GraphPad Prism. Fisher's exact test for significance of differentially expressed pathways in transcriptomic data were performed using IPA software. Throughout the study, p < 0.05 was defined as the threshold for significance.

DATA AND CODE AVAILABILITY

The accession number for the microarray data reported in this paper is: GEO: GSE136157. The accession number for the RNA-Seq data reported in this paper is: GEO: GSE136300. The accession number for the ChIPSeq data reported in this paper is: GEO: GSE136205.